

# An experimental evaluation of Siamese Neural Networks for robot localization using omnidirectional imaging in indoor environments

Juan José Cabrera<sup>1\*</sup>, Vicente Román<sup>1</sup>, Arturo Gil<sup>1</sup>, Oscar Reinoso<sup>1,2</sup> and Luis Payá<sup>1</sup>

<sup>1</sup>Institute for Engineering Research (I3E), Miguel Hernández University, Elche, Spain.

<sup>2</sup>Valencian Graduate School and Research Network for Artificial Intelligence (valgrAI), Spain.

\*Corresponding author(s). E-mail(s): [juan.cabreram@umh.es](mailto:juan.cabreram@umh.es);

## Abstract

The objective of this paper is to address the localization problem using omnidirectional images captured by a catadioptric vision system mounted on the robot. For this purpose, we explore the potential of Siamese Neural Networks for modeling indoor environments using panoramic images as the unique source of information. Siamese Neural Networks are characterized by their ability to generate a similarity function between two input data, in this case, between two panoramic images. In this study, Siamese Neural Networks composed of two Convolutional Neural Networks (CNNs) are used. The output of each CNN is a descriptor which is used to characterize each image. The dissimilarity of the images is computed by measuring the distance between these descriptors. This fact makes Siamese Neural Networks particularly suitable to perform image retrieval tasks. First, we evaluate an initial task strongly related to localization that consists in detecting whether two images have been captured in the same or in different rooms. Next, we assess Siamese Neural Networks in the context of a global localization problem. The results outperform previous techniques for solving the localization task using the COLD-Freiburg dataset, in a variety of lighting conditions, specially when using images captured in cloudy and night conditions.

**Keywords:** Localization, Omnidirectional Imaging, Holistic description, Mobile robots, Siamese Neural Network.

## 1 Introduction

During the past few years, vision sensors have been used extensively in the field of map building and localization with mobile robots (Hu et al., 2020; Zhong et al., 2018). In particular, the ability to localize in the map is of paramount importance in order to develop autonomous robots that can navigate in real operation conditions (Reinoso and Payá, 2020). The interest in using vision sensors to capture information from the environment is still high. Cameras can capture a big amount of information from the environment with a relatively low cost and they can be used in both, indoor and outdoor areas. Additionally, the images permit carrying out other highly specialized tasks such as object recognition and people detection.

Among the available configurations to capture visual information, the use of omnidirectional vision sensors in mobile robotics has become common. Omnidirectional cameras obtain images that cover a field of view of 360 *deg.* around the robot (Junior et al., 2016). As a result, they are commonly used to address navigation tasks (Rituerto et al., 2010).

The large amount of information provided by cameras requires robust techniques to extract and describe the relevant visual information. Different paradigms have been considered to extract this relevant information. A first group of techniques concentrate on detecting, describing and tracking some landmarks or local features along the scenes (Garcia-Fidalgo and Ortiz, 2015; Luthardt et al., 2018; Shamsfakhr et al., 2019; Cao et al., 2020; Lin et al., 2020). Different local features have been used in mapping and localization tasks, including SIFT, SURF (Gil et al., 2010) and ORB descriptors (E. Rublee and Bradski, 2011). A global description of each image can then be obtained, for example, by means of the Bag of Words model (Raúl Mur-Artal and Tardós, 2015). A second group of techniques work with each scene as a whole, and build a unique descriptor per image that contains information on its global appearance (Berenguer et al., 2015; Korrapati and Mezouar, 2017; Khaliq et al., 2019; Liu and Zhang, 2012). Finally, hardware developments have led many authors to use Artificial Intelligence (AI) techniques to extract relevant information from images. Specifically, Convolutional Neural Networks (CNNs) have been proposed to address different computer vision and robotics tasks. For example, Xu et al. (2019) and Leyva-Vallina et al. (2019) proposed global appearance descriptors based on a CNN to obtain the most probable pose of the robot.

In general terms, holistic description methods lead to maps in which a set of robot poses and their associated descriptors are stored. In this way, each pose of the robot is represented by a holistic descriptor and this representation leads to straightforward localization algorithms, based on the pairwise comparison between descriptors.

In this manuscript we assess the usage of Siamese Neural Networks in the context of image description and robot localization. Siamese Neural Networks permit evaluating two images at the same time in such a way that they provide a similarity measurement at the output. Therefore, they have the potential to address visual recognition of places and estimate the position of a mobile robot. In the present paper, we evaluate this potential. The main contributions of this paper can be summarized as follows.

1. We explore the capability of Siamese Neural Networks for modeling indoor environments, using panoramic images as the unique source of information.
2. We train and evaluate Siamese Neural Networks with the purpose of detecting whether two images have been captured in the same or in different rooms.
3. We train Siamese Neural Networks capable of estimating robot position as a global image retrieval problem.
4. We conduct an exhaustive study on the influence of the Siamese Neural Networks' architecture and the most relevant parameters. Moreover, we analyze the robustness against some common visual phenomena that may occur in real operation conditions, such as changes of the lighting conditions or image blur.

## 2 State of the art

As stated before, Siamese Neural Networks are able to generate a similarity function from pairs of input data. They can be regarded as a superstructure that includes two Neural Networks. These architectures accept two different inputs and offer a single output. The underlying networks share the same weights and different functions can be used to conform a single output. They were first proposed in 1993 in order to distinguish correct signatures from forgeries (Bromley et al., 1993). Since then, these architectures have been proposed in different areas of knowledge. For example, Thiolliere et al. (2015) proposed a Siamese Neural Network for audio and speech signal processing, Zheng et al. (2019) used this architecture for the comparison of DNA sequences or Jeon et al. (2019) used it for drug discovery purposes. Furthermore, Parajuli et al. (2017) developed a Siamese Neural Network to track cardiac motion and Sandouk and Chen (2017) proposed a Siamese architecture in order to recognize music tags.

During the past few years, AI in general and CNNs in particular have been used in the field of mobile robotics for a variety of purposes. For instance, for *mapping* (Sinha et al., 2018; Moolan-Feroze et al., 2019; Brahmabhatt et al., 2018), *localization* (Weinzaepfel et al., 2019; Li et al., 2017; Cattaneo et al., 2019), *navigation* (Zhao et al., 2018; Ma et al., 2019) and *simultaneous localization and mapping* (Lu and Lu, 2019; Liu et al., 2019). A complete state-of-the-art review on mobile robotics tasks based on the use of AI can be found in (Cebollada et al., 2020). Other applications of AI in the context of mobile robotics include: *self-driving navigation* (Sharma et al., 2017; Polvara et al., 2018; Organisciak et al., 2020), *face detection and recognition* (Wang et al., 2017; Jiang and Wang, 2017; Hu et al., 2021), *object recognition and categorization* (Nozawa et al., 2021; Zaki et al., 2019; Feng et al., 2020) and *mapping and localization* (Tanzmeister et al., 2014; Holliday and Dudek, 2018; Ruan et al., 2019).

Convolutional Neural Networks (CNNs) are the most popular techniques among AI tools. Currently, they are used in many mapping and localization tasks due to their successful performance in many practical applications. They are designed to receive images as input and their structures are specially created to obtain descriptors that synthesize the information in them (Chollet et al., 2018). Therefore, they can be used to describe the global appearance of an image. In this sense, Cebollada et al. (2019) proposed holistic descriptors obtained with a CNN to perform localization within topological models, studying their strength against illumination variations. Also, Xu et al. (2019) and Leyva-Vallina et al. (2019) proposed these techniques to obtain the most probable robot position. Additionally, Ballesta et al. (2021) studied localization tasks using CNNs and regression layers as global appearance descriptors. Some well known architectures have been used as basic structures to develop new modified networks for robotic navigation purposes. AlexNet (Krizhevsky et al., 2012), VGG16 (Simonyan and Zisserman, 2014), GoogleNet (Szegedy et al., 2015) or NetVLAD (Arandjelovic et al., 2016) are some of them.

The Convolutional Neural Networks presented above can be used to form a Siamese Neural Network. In the field of robotics, they have been rarely used and some studies that proposed this structure in this field are mentioned below. For example, Utkin et al. (2017) use a Siamese Neural Network to support the security control of a robot by detecting anomalies in its behaviour and Zeng et al. (2018) present a robotic pick-and-place system capable of identifying and grasping both known and novel objects in cluttered environments using a Siamese Neural Network. Moreover, Li and Zhang (2019) use the VGG16 network to conform a Siamese structure for object detection and tracking. Additionally, Zhang and Peng (2019) presented a study in which Siamese Networks are followed by Fully Connected layers or Region Proposal Network structures in the context of real-time visual tracking.

Regarding robot localization tasks, Leyva-Vallina *et al.* have proposed the use of Siamese Neural Networks to address the place recognition problem in garden environments (Leyva-Vallina et al., 2019, 2021). Moreover, this architecture has been proposed for localization using LiDAR scans (Yin et al., 2018; Chen et al., 2022).

In the present paper, we address the localization of a mobile robot using panoramic images in such a way that we study in detail different architectures and training configurations of Siamese Neural Networks. For this purpose, we propose as an initial approach to train and test the capability of the network to distinguish between images captured in the same and different rooms. In addition, in this study we also tackle the global localization problem using Siamese Neural Networks.

### 3 Siamese Neural Networks

Siamese Neural Networks can be described as a superstructure that includes, at least, two different Neural Networks beneath. Weights are shared between the networks and a single output is generated by combining the outputs of both networks. Figure 1 shows a general representation of a Siamese Neural Network architecture. In the present work, we use Convolutional Neural Networks to conform the two branches of the Siamese Neural Network. The output of each CNN is a descriptor which is used to characterize each input image. The dissimilarity of the input images is computed by measuring the distance between these descriptors. In this way, Siamese Neural Networks can be trained to generate similar descriptors when the training images belong to the same category. This fact makes Siamese Neural Networks particularly suitable to perform image retrieval tasks. Additionally, it is worth noting that the outputs, training, and performance of the network depend directly on:

- The architectures used in subnetworks W1 and W2 to extract the main features of the images.
- The conversion of the feature maps from the convolutional layers to a descriptor vector.
- The dimension of the output descriptors that embed the pair of input images.
- The training carried out with the available images. In particular, the labelling and the ratio of images of each category.

In this manuscript, we analyze the influence of these items on the visual localization of the robot.

### 4 Visual Localization

This section is focused on explaining the mobile robot localization using visual information. In this manuscript, we assume that a visual map of the environment is initially available. To obtain this map, the robot has

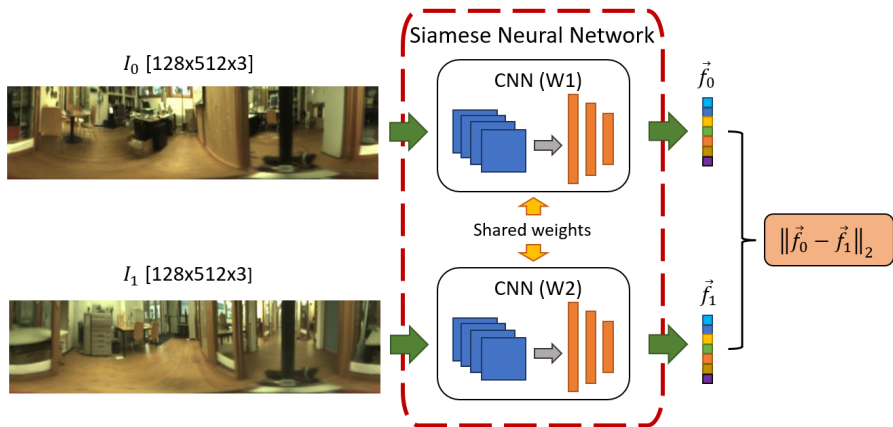


**Fig. 1** Representation of the architecture of a general Siamese Neural Network.

moved throughout the area capturing omnidirectional images along the trajectory. Firstly, the images are transformed to a panoramic format (with size  $128 \times 512$  in the present work), resulting in the set  $\{I_1, I_2, \dots, I_N\}$ . These images are captured from  $N$  points of view, whose poses are known and stored  $\vec{P}_i = (x_i, y_i, \theta_i)$ ,  $i = 1, \dots, N$ . Additionally the room where the picture has been captured is known too, so a set of labels is available:  $\vec{R}_i = (r_i)$ ,  $i = 1, \dots, N$ . Each image will be embedded into a single descriptor during the localization, using the proposed architecture, yielding  $\{\vec{f}_1, \vec{f}_2, \dots, \vec{f}_N\}$ . The trajectory followed by the robot includes different rooms with different visual information. In this work, these rooms include a corridor, some offices, a library and a bathroom.

Taking these facts into account, the initial map is composed by the set of images, their poses and the room in which the images are captured  $\{(I_1, \vec{P}_1, r_1), (I_2, \vec{P}_2, r_2), \dots, (I_N, \vec{P}_N, r_N)\}$ . Using this information, some Siamese Neural Networks are trained to address localization.

## 4.1 Room Discrimination

In this subsection an initial task related to localization is evaluated to study whether a Siamese Neural Network is able to distinguish between images captured from the same or from different rooms. For this purpose, the model will be trained and tested with pairs of random images captured from the same and/or different room.

## 4.2 Global Localization

In this study we consider that a map of the environment is available, as described before. The absolute localization problem is solved by comparing the test image directly with all the images in the map. This comparison is performed using the descriptors  $\vec{f}_i$  associated to each image in the map. The pose

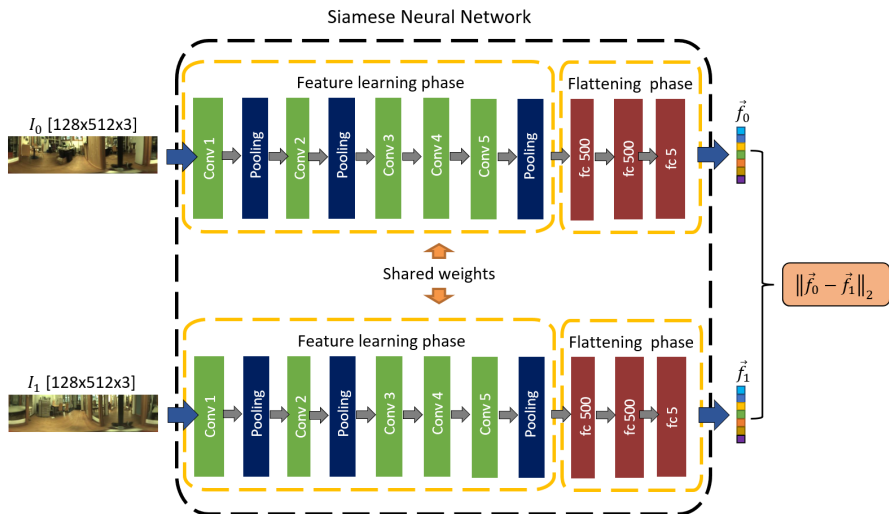


**Fig. 2** Detailed representation of a Siamese Neural Network with AlexNet in the feature learning phase and the flattening phase composed of three fully connected layers.

of the robot is found as the most similar descriptor contained in that map. The problem is approached with pure visual information and assuming that no information about the previous pose of the robot is available.

## 5 Architecture and Training of the Deep Learning tools

The structure of a classical CNN used for classification tasks can be split into two different stages (Cebollada et al., 2019): the feature learning and the classification stages. Features are extracted using several convolutional layers whereas the classification task can be constructed using fully connected layers and a final Softmax function. In our approach, the classification stage is replaced by a flattening phase. In this sense, the feature learning phase outputs a feature map which is flattened to a vector and dimensionally reduced by fully connected layers. This phase permits generating a single description vector per input image. As a result, the model provides two vectors  $\vec{f}_0$  and  $\vec{f}_1$  (one per input image). These descriptors are compared using the Euclidean distance in the comparison phase ( $d(\vec{f}_0, \vec{f}_1) = \|\vec{f}_0 - \vec{f}_1\|_2$ ). This architecture is shown in Figure 2. Therefore, during training, the weights of the networks are updated in order to obtain the optimal global descriptors. After the comparison, the distance between them and the similarity label (1 : *dissimilar*, 0 : *similar*) are used as data for the loss function. In our case the loss function used is the Contrastive Loss Function.

$$L(\vec{f}_0, \vec{f}_1) = \frac{1}{2}(1 - y)d(\vec{f}_0, \vec{f}_1)^2 + y\frac{1}{2}\max(\alpha - d(\vec{f}_0, \vec{f}_1), 0)^2 \quad (1)$$

Where  $y$  is the similarity label and  $\alpha > 0$  is a margin. The margin defines a radius around the descriptor so that dissimilar pairs of images contribute to the loss function only if their distance is within this radius (Hadsell et al., 2006).

## 5.1 Parameters and Networks

In this manuscript we compare different networks in the feature learning stage. As inputs to the flattening layers we consider the representation computed in the last convolutional layer of Alexnet (Krizhevsky et al., 2012), DenseNet (He et al., 2016), VGG11, VGG13, VGG16 and VGG19 (Simonyan and Zisserman, 2014). In Table 1 the feature extraction layers of those CNNs are presented. Additionally two simple networks created with three conv2d layers are also evaluated (Table 2). The ReLU activation layers are not shown for brevity, but they have been used after each conv2d layer. The different feature learning structures are evaluated in the Section 6.

**Table 1** Configuration of the Feature Extraction Neural Networks. The ReLU activation layers have been omitted for brevity.

AlexNet	DenseNet	VGG11	VGG13	VGG16	VGG19
input (128 x 512 RGB image)					
conv2d-64	conv2d-112	conv2d-64	conv2d-64 conv2d-64	conv2d-64 conv2d-64	conv2d-64 conv2d-64
maxpool	maxpool	maxpool			
conv2d-192	conv2d-56 x 6	conv2d-128	conv2d-128 conv2d-128	conv2d-128 conv2d-128	conv2d-128 conv2d-128
maxpool	averagepool	maxpool			
conv2d-384 conv2d-256 conv2d-256	conv2d-28 x 12	conv2d-256 conv2d-256	conv2d-256 conv2d-256	conv2d-256 conv2d-256 conv2d-256	conv2d-256 conv2d-256 conv2d-256 conv2d-256
	averagepool	maxpool			
maxpool	conv2d-14 x 24	conv2d-512 conv2d-512	conv2d-512 conv2d-512	conv2d-512 conv2d-512 conv2d-512	conv2d-512 conv2d-512 conv2d-512 conv2d-512
	averagepool	maxpool			
	conv2d-7 x 16	conv2d-512 conv2d-512	conv2d-512 conv2d-512	conv2d-512 conv2d-512 conv2d-512	conv2d-512 conv2d-512 conv2d-512 conv2d-512
	averagepool	maxpool			
fc-500					
fc-500					
fc-5					

\* Blue color layers correspond to the flattening layers.

\*\*VGG networks have their Batch Normalize (bn) version where after each conv2d layer a BatchNorm2d layer normalizes the results.

**Table 2** Simple Convolutional Neural Networks without pretraining.

Simple 1	Simple 2
input (128 x 128 RGB image)	
conv2d-3	conv2d-3
conv2d-8	conv2d-16
conv2d-16	conv2d-32
maxpool	
fc-500	
fc-500	
fc-5	

\* Blue color layers correspond to the flattening layers.

We have also tested different structures in the flattening phase. As a global baseline three fully connected layers are used, but different versions are considered, with different number of neurons. The different layers used during the evaluation are presented in Table 3.

**Table 3** Configuration of the flattening phase in our approach.

version 1	version 2	version 3
fc-500	fc - 500	fc - 1000
fc - 500	fc - 100	fc - 1000
fc - 5	fc - 10	fc - 10

Other parameters are also tested during the training phase with the aim of obtaining the best Siamese Neural Network for our application. The hyper-parameters considered during the evaluation are the following: the batch size (number of samples processed before the model is updated), the epochs (number of complete passes through the training dataset) and the percentage of images (percentage of training pairs of images from the same or different rooms, so that the network can learn adequately similarities and dissimilarities between rooms). In the experiments, the learning rate is kept constant at 0.001 (rate of change of the model in response to the estimated error) and the momentum is 0.9 (contribution of the parameter update step of the previous iteration upon the current iteration).

## 5.2 Data Augmentation

Additionally, a data augmentation technique is proposed as a method to improve the performance of the network. It increases the number of images in the training dataset. Having a larger number of training images reduces the overfitting of the model and boosts its robustness against real operation conditions. Cabrera et al. (2021) and Sakkos et al. (2019) demonstrated the use of data augmentation in CNNs to improve their effectiveness under changing lighting conditions.

Our proposed data augmentation is focused mainly on such lighting conditions and concentrates on editing local regions by simulating lights, reflections

and shadow effects caused by light sources from different angles. Moreover global illumination changes are also taken into account. Other effects not related with the illumination but that can appear when images are captured in real operating conditions are also used.

**Local effects:** Light sources that fall on a specific area or the surface of an object are reproduced. We call this local illumination changes since only a small patch of the image is being affected. The shape of different light sources can vary meaningfully.

Circular shapes from light bulbs or square and trapezoid shapes from reflections or windows are common. We edit the intensity of different regions following these shapes to simulate the light source; the pixel intensity is increased to reproduce more bright or it is decreased to simulate a shadow effect. In order to replicate a realistic fading effect, the intensity of brightening/darkening is gradually decreased from the center to the edge as an attenuation of the light.

The size of the shapes and the position is selected randomly to simulate the effect in different ways and so does the maximum value to consider different intensities. In our experiments these figures are built with sizes between 15 and 40 pixels, different intensities are applied and the patch is degraded from intensity values  $\pm 160$  or 100 to 5. The effects and shapes are shown in the Figure 3.

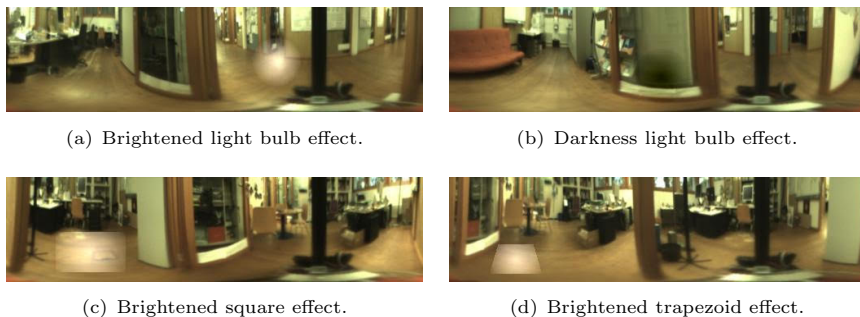


**Fig. 3** Individual local effects for data augmentation based on illumination.

**Global illumination:** Global illumination variations can occur in some cases. To model such illumination changes, we need to alter pixels across the whole image, rather than in a small region. A constant value  $c$  is added to all the pixels to model a global brightness effect on the image or it is subtracted to simulate a global darkness. The value of  $c$  varies from 35 to 75 in this work. Figures 4(b) and 4(c) show the effect.

**Sharpness/Blurring:** Finding sharper borders among diverse objects will contribute to provide a better separation among them and between foreground and background. In contrast, blurring effects are caused by low illumination and movements of the camera, which are common in mobile robotics. Both effects are incorporated in the data augmentation. They can be observed in Figures 4(d) and 4(e). Both can be achieved by a convolution operation using the following masks.

$$\begin{array}{cc}
 \text{Sharpness effect} & \text{Blurring effect} \\
 m_{sh} = \begin{bmatrix} 0 & -1 & 0 \\ -1 & 5 & -1 \\ 0 & -1 & 0 \end{bmatrix} & m_{bl} = \frac{1}{25} \begin{bmatrix} 1 & 1 & 1 & 1 & 1 \\ 1 & 1 & 1 & 1 & 1 \\ 1 & 1 & 1 & 1 & 1 \\ 1 & 1 & 1 & 1 & 1 \\ 1 & 1 & 1 & 1 & 1 \end{bmatrix}
 \end{array}$$

**Contrast variation:** The contrast of the image plays an important role in highlighting different objects in the scene. Low contrast images usually look softer and with less shadows and reflections. The effect is proposed for this data augmentation to improve the robustness of the framework. The contrast is modified following the next equation:

$$I_s = 64 + c * (I - 64)$$

where  $I_s$  is the resulting image,  $I$  the original image and  $c$  is the contrast factor. For  $c > 1$  the contrast increases and  $c < 1$  decreases the contrast. Additionally, an equalization of the image is also added to the data augmentation set. It evenly distributes the histogram values, which permits obtaining a new contrast augmentation effect. Figure 4(f) shows this effect.

**Saturation changes:** The colour saturation of the image deals with the intensity of the colour. The less saturation, the less colourful the image is, even it can resemble a grey-scale image if the saturation is very low. In contrast, more vivid colours are obtained when the colour saturation is high. It can simulate situations when illumination changes significantly. The colour saturation can be edited by converting the RGB image to HSV, after that, it is possible to directly change the saturation channel by multiplying it by a constant factor  $c$ . If the saturation attribute is multiplied by  $c > 1$  the colours become more saturated and by  $c < 1$  the colour saturation decreases. The effect can be seen in Figure 4(g).

**Rotation:** The original image covers 360 degrees around the robot. For that reason the image can be rotated without losing any piece of information. This effect will simulate the situation in which the robot is in the same position but the orientation is different. Moreover, having a training dataset containing this

type of effect is expected to provide the Neural Network with rotation invariance. Figure 4(h) shows a rotation effect of 115 degrees. Random rotations between 10 and 350 degrees are applied to the training images.

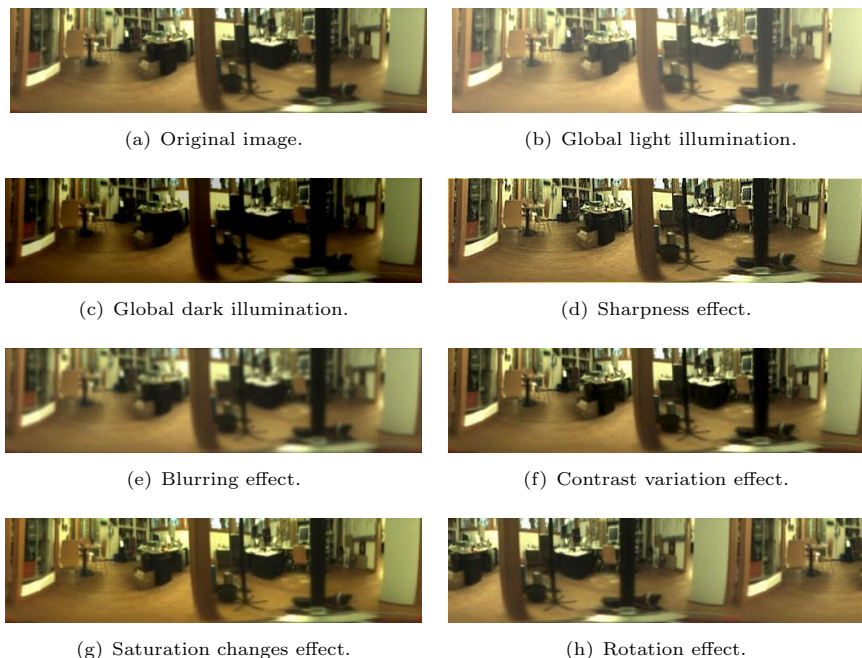


**Fig. 4** Global effects for data augmentation.

**Combined changes:** Additionally some effects are combined to obtain a larger data augmentation, but not all the effects are combined together. Global illumination and a single local effect are combined in all the possible variations, e.g. global darkness is combined with a brightening circle shape effect, global brightness is combined with a brightening trapezoidal effect, etc. Additionally, the local effects are also combined. The circle shape effect is combined with the square effect, the trapezoidal effect or another circle shape effect, the combinations can be brightened+brightened, brightened+darkness and darkness+darkness; the circle shape effect is also combined with other two circle shape effects, obtaining an image with three light bulb effects. Finally, the rotation effect is individually combined with all the effects and the combinations described above.

### 5.3 Training and testing the Siamese Neural Network

As presented in Section 5.1, different CNNs architectures can be used as the base of Siamese Neural Networks. Initially, we start from pretrained networks with known weights and biases. Then, we retrain the network to fit it to our

application. This transfer learning technique is well-known and has previously been used in mobile robotics (Cabrera et al., 2021; Cebollada et al., 2020).

The following Subsection 5.3.1 will address an initial task which consists in training and evaluating the capability of a Siamese Neural Network to identify whether two images were captured from the same or different rooms. Finally, in Subsection 5.3.2 we will detail the characteristics of the training and test to address the absolute localization problem with siamese architectures. Emphasis will be placed on the labelling required to perform the desired task.

### 5.3.1 Room Discrimination

The main goal of this task is to evaluate whether a Siamese Neural Network is capable of determining if two images belong to the same or different room. It is an important capability to perform localization tasks.

The *training phase* is performed by feeding the network with pairs of images. These pairs are labelled with 0 if they have been captured from the same room and 1 if not. The ratio same/different room pairs is varied in the *training phase* to study its influence.

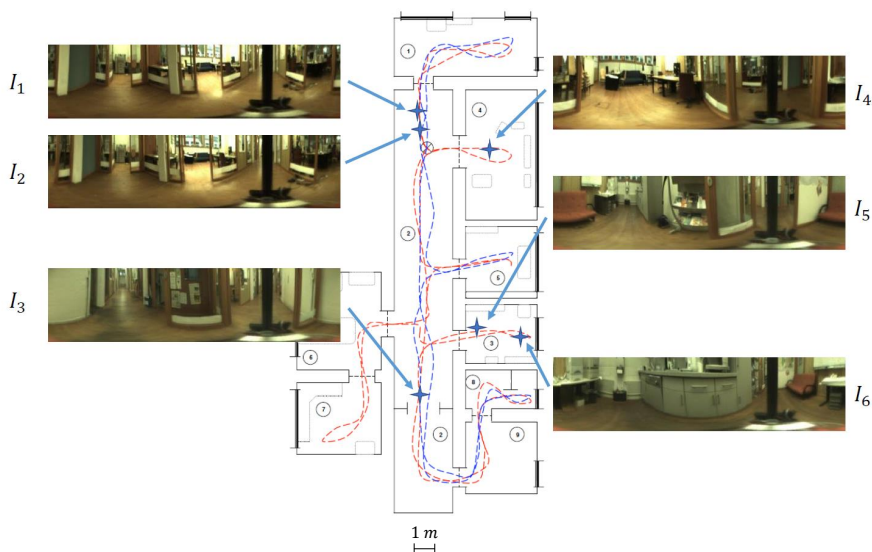


**Fig. 5** Example of different trajectories of the robot.

During the *test phase*, pairs of images are fed into the network. At the output, the network labels them with a number between 0 and 1; if the result is under 0.5 we interpret that the images have been captured from the same room. On the contrary, the images belong to different rooms. The images used to test the network are different from the training images, they are captured

in the same building but in different times, in a variety of lighting conditions. Also the trajectory followed by the robot to capture the test images is similar to the one used to capture the training images, but the images are captured from different robot poses (Figure 5).

### 5.3.2 Global localization

The global localization problem considers the estimation of the robot pose within the whole floor of the building. For this purpose, a Siamese Neural Network is trained. The *training* is carried out with image pairs labelled with the following equation:

$$Label(I_i, I_j) = \begin{cases} \frac{\|\vec{p}_i - \vec{p}_j\|_2}{K_b} & \text{if } I_i \text{ and } I_j \text{ belong to the same room} \\ 1 & \text{otherwise} \end{cases} \quad (2)$$

where  $I_i$  and  $I_j$  are two images and  $\vec{p}_i$  and  $\vec{p}_j$  are their corresponding positions (coordinates of the capture points). This constitutes a normalized Euclidean distance between the capture points.  $K_b$  corresponds to the maximum distance between two images in the building. Table 4 shows different examples according to Figure 5.

**Table 4** Example pairs and its label value for the absolute localization task. The labels of the images are shown in Figure 5.

Pair	Euclidean distance (m)	Label Value
$I_1 - I_2$	0.33	$\frac{0.33}{18.99} = 0.017$
$I_1 - I_3$	12.82	$\frac{12.82}{18.99} = 0.675$
$I_1 - I_4$	-	1
$I_1 - I_5$	-	1
$I_4 - I_5$	-	1
$I_5 - I_6$	2.48	$\frac{2.48}{18.99} = 0.131$

Where:

18.99 m is the maximum distance between two images in the target environment

Once the network has been trained, the test is performed by using the map which is composed by the set of image descriptors and their positions  $\{(\vec{f}_1, \vec{p}_1), (\vec{f}_2, \vec{p}_2), \dots, (\vec{f}_N, \vec{p}_N)\}$ . Each descriptor has been calculated by the trained Siamese Neural Network. The absolute localization is performed as a pairwise comparison between image descriptors. Given a test image  $I_t$ , the Siamese Neural Network outputs its corresponding descriptor  $\vec{f}_t$ . Finally, the position of the robot is estimated by selecting the pose associated to the descriptor in the map that minimizes the distance  $\|\vec{f}_t - \vec{f}_i\|_2$ , with  $i = 1, \dots, N$ .

## 6 Experiments

The set of experiments is designed to test the performance of the Siamese Neural Network as global descriptor generator to tackle the room discrimination

and global localization task as explained in subsections 5.3.1 and 5.3.2. Furthermore, the training and test datasets used in this research are presented in the following subsection.

## 6.1 Training and test datasets

The images used in the experiments are obtained from an indoor dataset (Pronobis and Caputo, 2009). This database was captured by an omnidirectional vision sensor mounted on a mobile robot which followed different trajectories that visited 9 different rooms. A variety of lighting conditions was considered to capture the sets of images.

Table 5 shows the number of images per room for each of the datasets used in this research. Two training sets are considered: training set 1 consists of 8486 images captured under cloudy, sunny and night illumination conditions (*COLD-Freiburg Part A Path 2 Cloudy 3*, *Freiburg Part A Path 2 Night 1*, *Freiburg Part A Path 2 Sunny 3*). Training set 2 has been obtained by applying a data augmentation to the cloudy sequence of training set 1, thus generating 977856 images. With respect to the test sets, four different sets are considered: test set 1 consists of 2595 images under cloudy lighting condition (*COLD-Freiburg Part A Path 2 Cloudy 2*), test set 2 contains images captured under night lighting condition and consists of 2707 images (*COLD-Freiburg Part A Path 2 Night 2*), test set 3 consists of 2114 images under sunny lighting condition (*COLD-Freiburg Part A Path 2 Sunny 2*) and test set 4 is composed of all the images in the previous test sets. It should be noted that the images in the test sets are different, in all cases, from the images that constitute the training sets. Finally, the visual map has been obtained after sampling the path under the cloudy lighting condition of the training set 1, obtaining a total of 556 images.

In this way, the training sets will be used to carry out the training of the Siamese Neural Networks, and the test sets will evaluate the performance of the networks under the three lighting conditions. The visual model is the map available for the robot to carry out the localization, so it will be used in the testing phase of the global localization.

## 6.2 Room Discrimination

In this subsection we assess the ability of the network to predict whether two images are taken from the same room. The effectiveness of the Siamese Neural Network is calculated by comparing pairs of images and checking their label. The results are expressed in percentage of accuracy. Several experiments have been conducted while varying different parameters: the feature extraction architecture, the flattening layers and the percentage of similar/dissimilar images. As common parameters, we train the network using 8486 pairs of

**Table 5** Summary of the training and test datasets. This table shows the number of images per room and the total of images of each dataset.

Room	Training dataset 1	Training dataset 2	Test dataset 1	Test dataset 2	Test dataset 3	Test dataset 4	Visual Map
<b>1P0-A</b>	518	76,736	218	168	123	509	44
<b>2P01-A</b>	694	82,016	233	215	187	635	46
<b>2P02-A</b>	428	55,616	158	168	109	435	31
<b>CR-A</b>	3,258	416,416	1,183	1,114	793	3,090	238
<b>KT-A</b>	674	80,608	229	270	213	712	46
<b>LO-A</b>	395	46,464	132	121	102	355	26
<b>PA-A</b>	804	99,968	284	241	191	716	57
<b>ST-A</b>	495	53,152	151	198	180	529	30
<b>TL-A</b>	619	66,880	190	212	216	618	38
<b>Total:</b>	8,486	977,856	2,595	2,707	2,114	7,416	556

images per epoch from the training dataset 1 and we use the Stochastic Gradient Descent (SGD) optimiser, with a learning rate of 0.001 and momentum of 0.9. Moreover, we test the network with 7000 pairs of images extracted from the test dataset 4.

### 6.2.1 Influence of the architecture on the feature extraction process

In this subsection we compare different models in the feature extraction stage of a Siamese Neural Network. The different models used can be observed in Table 1. The training has been performed using a batch size of 256 and 5 epochs. During training, the dataloader presents a 50% of images from the same room and a 50% of images from the different rooms. During these experiments, the flattening is performed with 3 fully connected layers composed by 500-500-5 neurons in each.

Results are presented in Table 6 in terms of global accuracy. Additionally, the test accuracy for the same and different room predictions is also presented. The table shows that the best networks are VGG13 and VGG16. They obtain the best accuracy for predicting pairs of images in the same room (99.44% and 99.47% respectively). In addition, VGG13 and VGG16 present the best accuracy predicting if two images are taken from different rooms (79.86% and 78.91%). Moreover, the ‘Simple 1’ and ‘Simple 2’ networks obtain considerably good results using only three convolutional layers. Finally, in general terms, it can be observed that all the architectures perform better in predicting whether two images belong to the same room. For this reason, we consider below the possibility of varying the percentage of images of each category in the training phase.

### 6.2.2 Influence of the training parameters

In the light of the previous results, next, different training parameters are evaluated. As we explain in the previous subsection, the ratio of training pairs

**Table 6** Accuracy using different Feature Extraction Neural Networks.

Network	Global Test Accuracy	Same Room Accuracy	Different Room Accuracy
Simple 1	<b>84.59%</b>	98.16%	<b>71.03%</b>
Simple 2	86.45%	98.87%	74.06%
Alexnet	86.10%	98.78%	<b>73.41%</b>
Densenet	86.06%	97.61%	74.52%
VGG11	87.43%	99.08%	75.78%
VGG11bn	87.51%	97.49%	77.53%
VGG13	<b>89.65%</b>	<b>99.44%</b>	<b>79.86%</b>
VGG13bn	88.52%	98.26%	78.77%
VGG16	<b>89.19%</b>	<b>99.47%</b>	<b>78.91%</b>
VGG16bn	<b>82.04%</b>	<b>92.68%</b>	73.39%
VGG19	89.17%	99.30%	79.04%
VGG19bn	86.58%	<b>95.52%</b>	77.64%

of images in each category is expected to have a substantial influence upon the results. In consequence, we propose to change the percentage of pairs of images at the training phase. The percentage of images taken from the same and different rooms varies from 5% to 40% and from 95% to 60% respectively. For brevity, we only show the results obtained with VGG13, VGG16 and AlexNet networks. The rest of the training parameters is tuned as before, using 256 as batch size and a flattening phase with three fully connected layers composed by 500, 500 and 5 neurons. The results are presented in Tables 7, 8 and 9. They show a correlation between the percentage of images of same/different room and its respective accuracy, i. e., when the percentage of pairs of images in the same room increases, its associated accuracy also does and a similar phenomenon occurs with the different room category.

**Table 7** Accuracy of **VGG13**. The table presents a variation in the total number of images and in the same-different ratios of training images.

Epoch	Percentage of Training Images (same-different)	Number of Training Images (same-different)	Global Accuracy	Same Room Accuracy	Different Room Accuracy
7	5%-95%	3,046-57,882	<b>89.88%</b>	<b>92.03%</b>	87.73%
9	5%-95%	3,917-74,419	91.89%	92.51%	91.27%
11	5%-95%	4,787-90,957	92.20%	92.71%	<b>91.70%</b>
7	10%-90%	6,093-54,835	92.72%	98.13%	87.30%
9	10%-90%	7,834-70,502	94.76%	98.69%	90.82%
11	10%-90%	9,574-86,170	<b>95.08%</b>	98.90%	91.25%
7	25%-75%	15,232-45,696	93.10%	99.09%	<b>87.12%</b>
9	25%-75%	19,584-58,752	93.46%	99.06%	87.86%
11	25%-75%	23,936-71,808	93.53%	<b>99.21%</b>	87.85%

Until this moment, all the experiments have been performed using 256 as batch size, but other values have been tested in order to check the best configuration. Tables 10 and 11 show the accuracy using different batch sizes. They show that the global accuracy increases when the batch size is lower.

**Table 8** Accuracy of **VGG16**. The table presents a variation in the total number of images and in the same-different ratios of training images.

Epoch	Percentage of Training Images (same-different)	Number of Training Images (same-different)	Global Accuracy	Same Room Accuracy	Different Room Accuracy
7	5%-95%	3,046-57,882	94.35%	96.47%	92.23%
9	5%-95%	3,917-74,419	94.94%	96.48%	93.39%
11	5%-95%	4,787-90,957	94.24%	97.77%	90.72%
7	10%-90%	6,093-54,835	93.04%	97.16%	88.92%
9	10%-90%	7,834-70,502	94.26%	97.18%	91.35%
11	10%-90%	9,574-86,170	93.59%	97.96%	89.22%
7	25%-75%	15,232-45,696	92.46%	99.21%	85.71%
9	25%-75%	19,584-58,752	92.28%	99.30%	85.25%
11	25%-75%	23,936-71,808	91.78%	98.81%	84.74%
7	40%-60%	24,371-36,557	92.95%	99.38%	86.52%
9	40%-60%	31,334-47,002	92.72%	99.48%	85.95%
11	40%-60%	38,298-57,446	93.28%	99.50%	87.05%

**Table 9** Accuracy of **AlexNet**. The table presents a variation in the total number of images and in the same-different ratios of training images.

Epoch	Percentage of Training Images (same-different)	Number of Training Images (same-different)	Global Accuracy	Same Room Accuracy	Different Room Accuracy
7	5%-95%	3,046-57,882	92.36%	90.11%	94.60%
11	5%-95%	4,787-90,957	93.58%	94.08%	93.07%
14	5%-95%	6,093-115,763	93.68%	94.14%	93.22%
7	10%-90%	6,093-54,835	92.05%	94.65%	89.44%
11	10%-90%	9,574-86,170	93.41%	96.84%	89.98%
14	10%-90%	12,186-109,670	93.01%	97.19%	88.82%
7	25%-75%	15,232-45,696	90.91%	97.54%	84.28%
11	25%-75%	23,936-71,808	91.16%	98.92%	83.39%
14	25%-75%	30,464-91,392	90.59%	98.28%	82.19%
7	40%-60%	24,371-36,557	88.33%	98.80%	77.85%
11	40%-60%	38,298-57,446	88.65%	99.07%	78.23%
14	40%-60%	48,742-73,114	88.54%	99.25%	77.82%

These tables show that relatively good performances can be achieved with some configurations. Notwithstanding that, we observe that in general terms, the same-room accuracy tends to decrease when the different-room accuracy increases and vice versa. This will be analyzed deeply in future works, but it may be due to the use of the Contrastive Loss function (Sun et al., 2020a).

### 6.2.3 Influence of the architecture of the flattening layers

As explained in subsection 5.1, the feature extraction layers output a matrix that is transformed to a vector in the flattening phase. Different combinations of fully connected layers are also evaluated. All these experiments have been performed training the network with a 10% of pairs of images taken from the same room and a 90% of pairs of images from different rooms.

Tables 12 and 13 show the results using 3 different combinations of fully connected layers. Each variation is described in Table 3. Similar results are

**Table 10** Accuracy using VGG16 and different batch sizes.

Batch Size	Epoch	Percentage of Training Images (same-different)	Global Accuracy	Same Room Accuracy	Different Room Accuracy
256	7	5%-95%	94.35%	96.47%	92.23%
256	11	5%-95%	94.24%	97.77%	90.72%
256	7	10%-90%	93.04%	97.16%	88.92%
256	11	10%-90%	93.59%	97.96%	89.22%
256	7	25%-75%	92.46%	99.21%	85.71%
256	11	25%-75%	91.78%	98.81%	84.74%
16	7	5%-95%	95.50%	98.26%	92.74%
16	11	5%-95%	93.84%	98.83%	88.85%
16	7	10%-90%	93.77%	98.13%	89.41%
16	11	10%-90%	94.42%	98.80%	90.05%
16	7	25%-75%	94.77%	99.15%	90.39%
16	11	25%-75%	94.08%	99.15%	89.00%

**Table 11** Accuracy using AlexNet and different batch sizes.

Batch Size	Epoch	Percentage of Training Images (same-different)	Global Accuracy	Same Room Accuracy	Different Room Accuracy
256	7	5%-95%	89.76%	90.11%	94.60%
256	11	5%-95%	93.58%	94.08%	93.07%
256	7	10%-90%	93.77%	98.13%	89.41%
256	11	10%-90%	94.42%	98.80%	90.05%
256	7	25%-75%	90.91%	97.54%	84.28%
256	11	25%-75%	91.16%	98.92%	83.39%
16	7	5%-95%	94.64%	96.25%	93.02%
16	11	5%-95%	95.24%	98.25%	92.24%
16	7	10%-90%	95.06%	98.87%	91.25%
16	11	10%-90%	95.07%	98.92%	91.22%
16	7	25%-75%	94.76%	99.10%	90.42%
16	11	25%-75%	94.60%	99.26%	89.94%

**Table 12** Accuracy using VGG16 and different flattening layers.

Flattening layers	Batch Size	Epoch	Global Accuracy	Same Room Accuracy	Different Room Accuracy
500-500-5	16	7	93.77%	98.13%	89.41%
500-500-5	16	11	94.42%	98.80%	90.05%
500-500-5	16	14	94.75%	99.10%	90.39%
500-100-10	16	7	95.76%	98.92%	92.60%
500-100-10	16	11	95.98%	99.11%	92.86%
500-100-10	16	14	95.44%	99.18%	91.70%
1000-1000-10	16	7	96.16%	98.90%	93.41%
1000-1000-10	16	11	95.63%	99.10%	92.16%
1000-1000-10	16	14	95.27%	99.10%	91.44%

obtained with the 3 different variations. The best result is obtained with 3 fully connected layers with 1000-1000-10 neurons each. Finally, if we analyse jointly all the results of the room discrimination experiment, the best result is obtained using VGG16 as the feature extraction network, 3 fully connected

**Table 13** Accuracy using **AlexNet** and different flattening layers.

Flattening layers	Batch Size	Epoch	Global Accuracy	Same Room Accuracy	Different Room Accuracy
500-500-5	16	7	93.77%	98.13%	89.41%
500-500-5	16	11	94.42%	98.80%	90.05%
500-500-5	16	14	93.84%	98.68%	88.99%
500-100-10	16	7	95.31%	98.20%	92.42%
500-100-10	16	11	95.41%	98.98%	91.83%
500-100-10	16	14	95.10%	99.06%	91.15%
1000-1000-10	16	7	95.36%	98.72%	91.99%
1000-1000-10	16	11	94.66%	98.59%	90.74%
1000-1000-10	16	14	95.28%	99.12%	91.43%

layers (1000-1000-10), 7 epoch and a batch size of 16; with this configuration 96.16% global accuracy is obtained: 98.90% same room accuracy and 93.41% different room accuracy.

### 6.3 Global Localization

The global localization is performed as explained in subsection 5.3.2. The VGG16 network is employed in this task since it led to the best results in the room discrimination task. Different experiments have been performed in order to choose the best configuration. We will mainly analyze the ratio of same/different room pairs, which is the parameter that has shown the greatest influence on the results. Moreover, in this subsection we will assess the influence of the data augmentation on the results. Each pair of images is labelled according the Equation 2.

First, concerning the experiment to evaluate the influence of the ratio same/different room pairs, we train the network using 8,486 pairs of images per epoch from the training dataset 1. Second, with respect to the experiment to assess the effect of the data augmentation, 977,856 pairs of images per epoch from the training dataset 2 are used. These two experiments are described in subsection 6.3.1. In both cases, the flattening layers are configured with 500-500-5 neurons. Moreover, subsection 6.3.2 evaluates the influence of the flattening layers. In this case, the training dataset 1 is used. As common parameters, we use 16 as batch size, the Stochastic Gradient Descent (SGD) optimizer, with a learning rate of 0.001 and a momentum of 0.9 and 30 epochs.

#### 6.3.1 Influence of the training parameters

##### *Ratio of same/different room pairs:*

Table 14 shows the results using VGG16 in the feature extraction part and three fully connected layers with 500-500-5 neurons in the flattening part. The training of the model has been performed with different percentages of pairs of images belonging to the same and different rooms. The results show that the lowest localization error is obtained when the training is performed using

40% of images from the same room and 60% of images from different rooms. Studying the results, as a general rule, training with a large percentage of image pairs from the same room deteriorates the localization error.

**Table 14** Average localization error (m) with **VGG16**. The table presents the global localization results with variations in the same-different ratio of training image pairs.

Feature extraction net	Percentage of Training Images (same-different)	Global Error	Cloudy Error	Night Error	Sunny Error
VGG16	80%-20%	0.6284 m	0.1826 m	0.5600 m	0.8023 m
VGG16	70%-30%	0.6035 m	0.1753 m	0.5375 m	0.7706 m
VGG16	60%-40%	0.6006 m	0.1802 m	0.4991 m	0.8649 m
VGG16	50%-50%	0.5821 m	0.1747 m	0.4837 m	0.8383 m
VGG16	40%-60%	0.5097 m	0.1481 m	0.4547 m	0.6508 m
VGG16	30%-70%	0.5193 m	0.1518 m	0.4908 m	0.6630 m
VGG16	20%-80%	0.5202 m	0.1521 m	0.4917 m	0.6642 m

### Data Augmentation:

Next, we evaluate the influence of the data augmentation on the localization task. Table 15 presents the results using the training dataset 2 (augmented) and test datasets 1, 2 and 3. For this purpose, we will start from the best configurations obtained so far and show the results according to the percentage of training image pairs.

**Table 15** Average localization error (m) with **VGG16** and data augmentation. The table presents the global localization results with variations in the same-different ratio of training image pairs.

Feature extraction net	Epochs	Percentage of Training Images (same-different)	Cloudy Error	Night Error	Sunny Error
VGG16	1	50%-50%	0.0630 m	0.4682 m	1.1880 m
VGG16	1	40%-60%	0.0608 m	0.4682 m	1.2703 m
VGG16	4	50%-50%	0.0375 m	0.3961 m	1.8257 m
VGG16	4	40%-60%	0.0407 m	0.4028 m	1.3733 m
VGG16	11	50%-50%	0.0440 m	0.3591 m	1.2264 m
VGG16	11	40%-60%	0.0418 m	0.3176 m	1.0050 m
VGG16	21	50%-50%	0.0375 m	0.2675 m	1.051 m
VGG16	21	40%-60%	0.0325 m	0.2573 m	0.9913 m

### 6.3.2 Influence of the architecture of the flattening layers

To conclude the experimental section, Table 16 shows the results after evaluating different flattening layers. In this case, a descriptor of dimension 5 works better in the global localization problem. The Siamese Neural Network is able to perform the localization with an average error of 0.5821 *m* when using as the flattening layers three different fully connected layers with 500, 500 and 5 neurons.

**Table 16** Average localization error (m) with **VGG16** and different configurations of the flattening layers.

Feature extraction net	Flattening layers	Epoch	Percentage of Training Images (same-different)	Global Error
VGG16	500-500-5	30	50%-50%	<b>0.5821 m</b>
VGG16	1000-1000-10	30	50%-50%	0.5904 m
VGG16	4096-4096-1000	30	50%-50%	<b>0.8313 m</b>

### 6.3.3 General comparison with other methods

Finally, the Siamese Neural Networks are compared with other previous global-appearance techniques which include the use of a single AlexNet structure and two classic analytic descriptors: HOG and gist, as described in the work by Cebollada et al. (2022). Table 17 compares all the methods in a global localization task using, in all cases, the COLD-Freiburg Dataset. As we can notice, the best results in terms of localization error for cloudy and night conditions are obtained with the siamese structures proposed in the present work. The best results for the sunny illumination condition are obtained first with the single Alexnet structure and second with the siamese network without data augmentation.

**Table 17** Comparison with other methods.

Global-Appearance Descriptor Technique	Cloudy Error	Night Error	Sunny Error
Alexnet (Cebollada et al., 2022)	0.0509 m	0.2880 m	<b>0.3894 m</b>
Siamese Network (ours)	0.1481 m	0.4547 m	0.6508 m
Siamese Network + DA (ours)	<b>0.0325 m</b>	<b>0.2573 m</b>	<b>0.9913 m</b>
HOG (Cebollada et al., 2022)	<b>0.1634 m</b>	0.4509 m	0.8198 m
gist (Cebollada et al., 2022)	0.0519 m	<b>1.065 m</b>	0.8839 m

## 7 Conclusions

In this paper, a global localization method using Siamese Neural Networks has been proposed and evaluated. Localization, along with mapping, is one of the main tasks to be addressed by an autonomous mobile robot. First, an initial task of discriminating same and different rooms has been proposed in order to assess the ability of Siamese Neural Networks and know the influence of the most relevant parameters. After that, the global localization problem is addressed.

In the experiments, several well known architectures have been tested to conform the Siamese Neural Network, some of which are AlexNet, VGG11, VGG13, VGG16, VGG19, VGG11bn, VGG13bn, VGG16bn and VGG19bn. The best performance in the initial task has been achieved by VGG13 and

VGG16. In general terms, the VGG architectures have provided the best results.

Apart from these feature extraction architectures, a group of Fully Connected layers have been added to carry out the conversion of the activation maps resulting from the convolutional layers to a description vector. In the present work, different sizes of the Fully Connected layers have been studied, as well as the size of the final descriptor. For the initial task, the performance of the network is slightly higher when the Fully Connected layers sizes are 1000-1000-10. In contrast, in the global localization, the localization error decreases drastically in those networks that have a set of Fully Connected layers of size 500-500-5 neurons.

The training parameter that contributes most to the performance of the network is the percentage of image pairs belonging to the same and different rooms. In this sense, there is a correlation between the percentage of images of same/different room and its respective accuracy, i.e., when the percentage of pairs of images in the same room increases, its associated accuracy also does and a similar effect occurs with the different room category. Furthermore, when the same room accuracy increases, the different room accuracy decreases, and vice versa. This situation may be caused by the Contrastive Loss function which has an associated lack of flexibility in the optimization. Other loss functions used in other applications could improve localization results, such as Circle Loss (Sun et al., 2020b) and will be considered in future studies.

In addition, a data augmentation technique has been proposed in order to improve the performance of the network. The proposed effects try to simulate real operation conditions. In addition, a set of effects specially designed to increase the robustness against changes of the lighting conditions in the scene have been generated. As for the results obtained, the performance of the network is especially benefited when working in cloudy and night lighting conditions. In the case of the cloudy lighting condition, when the training is performed with data augmentation, the average localization error is reduced around 12 centimeters. As for the night illumination condition, the average error is reduced around 20 centimeters. On the contrary, in sunny illumination condition the average localization error increases 34 centimeters when data augmentation is used.

As future works, the proposed localization techniques will be extended to outdoor environments, which are more challenging because of their unstructured and changing conditions. In addition, other types of sensors will be considered to carry out the localization robustly, such as LiDAR.

## Acknowledgements

The Ministry of Science, Innovation and Universities (Spain) has supported this work through “Ayudas para la Formación de Profesorado Universitario” (FPU21/04969). This work is also part of the project TED2021-130901B-I00, funded by MCIN/AEI/10.13039/501100011033 and by the European Union “NextGenerationEU”/PRTR, and of the project PID2020-116418RB-I00 funded by MCIN/AEI/10.13039/501100011033.

## References

- Arandjelovic, R., P. Gronat, A. Torii, T. Pajdla, and J. Sivic 2016. NetVLAD: CNN architecture for weakly supervised place recognition. In Proceedings of the IEEE conference on computer vision and pattern recognition, pp. 5297–5307.
- Ballesta, M., L. Payá, S. Cebollada, O. Reinoso, and F. Murcia. 2021. A CNN regression approach to mobile robot localization using omnidirectional images. Applied Sciences 11(16): 7521 .
- Berenguer, Y., L. Payá, M. Ballesta, and O. Reinoso. 2015. Position estimation and local mapping using omnidirectional images and global appearance descriptors. Sensors 15(10): 26368–26395 .
- Brahmbhatt, S., J. Gu, K. Kim, J. Hays, and J. Kautz 2018. Geometry-aware learning of maps for camera localization. In Proceedings of the IEEE Conference on Computer Vision and Pattern Recognition, pp. 2616–2625.
- Bromley, J., I. Guyon, Y. LeCun, E. Säckinger, and R. Shah. 1993. Signature verification using a “siamese” time delay neural network. Advances in neural information processing systems 6 .
- Cabrera, J.J., S. Cebollada, L. Payá, M. Flores, and Ó. Reinoso 2021. A robust CNN training approach to address hierarchical localization with omnidirectional images. In ICINCO, pp. 302–310.
- Cao, L., J. Ling, and X. Xiao. 2020. Study on the influence of image noise on monocular feature-based visual SLAM based on FFDNet. Sensors 20(17): 4922 .
- Cattaneo, D., M. Vaghi, A.L. Ballardini, S. Fontana, D.G. Sorrenti, and W. Burgard 2019. Cmrnet: Camera to lidar-map registration. In 2019 IEEE Intelligent Transportation Systems Conference (ITSC), pp. 1283–1289. IEEE.
- Cebollada, S., L. Payá, M. Flores, A. Peidró, and O. Reinoso. 2020. A state-of-the-art review on mobile robotics tasks using artificial intelligence and

visual data. Expert Systems with Applications: 114195 .

Cebollada, S., L. Payá, M. Flores, V. Román, A. Peidró, and Ó. Reinoso 2020. A deep learning tool to solve localization in mobile autonomous robotics. In ICINCO, pp. 232–241.

Cebollada, S., L. Payá, X. Jiang, and O. Reinoso. 2022. Development and use of a convolutional neural network for hierarchical appearance-based localization. Artificial Intelligence Review 55(4): 2847–2874 .

Cebollada, S., L. Payá, V. Román, and O. Reinoso. 2019. Hierarchical localization in topological models under varying illumination using holistic visual descriptors. IEEE Access 7: 49580–49595 .

Chen, X., T. Låbe, A. Milioto, T. Röhling, J. Behley, and C. Stachniss. 2022. Overlapnet: a siamese network for computing lidar scan similarity with applications to loop closing and localization. Autonomous Robots 46(1): 61–81 .

Chollet, F. et al. 2018. Deep learning with Python, Volume 361. Manning New York.

E. Rublee, V. Rabaud, K.K. and G. Bradski 2011. ORB: An efficient alternative to SIFT or SURF. In IEEE Int. Conf. on Computer Vision, pp. 2564—2571.

Feng, Q., H.P. Shum, and S. Morishima. 2020. Resolving hand-object occlusion for mixed reality with joint deep learning and model optimization. Computer Animation and Virtual Worlds 31(4-5): e1956 .

Garcia-Fidalgo, E. and A. Ortiz. 2015. Vision-based topological mapping and localization by means of local invariant features and map refinement. Robotica 33(7): 1446–1470 .

Gil, A., O.M. Mozos, M. Ballesta, and O. Reinoso. 2010. A comparative evaluation of interest point detectors and local descriptors for visual SLAM. Machine Vision and Applications. <https://doi.org/10.1007/s00138-009-0195-x> .

Hadsell, R., S. Chopra, and Y. LeCun 2006. Dimensionality reduction by learning an invariant mapping. In 2006 IEEE Computer Society Conference on Computer Vision and Pattern Recognition (CVPR'06), Volume 2, pp. 1735–1742. IEEE.

He, K., X. Zhang, S. Ren, and J. Sun 2016. Deep residual learning for image recognition. In Proceedings of the IEEE conference on computer vision and pattern recognition, pp. 770–778.

- Holliday, A. and G. Dudek 2018. Scale-robust localization using general object landmarks. In 2018 IEEE/RSJ International Conference on Intelligent Robots and Systems (IROS), pp. 1688–1694. IEEE.
- Hu, S., H.P. Shum, X. Liang, F.W. Li, and N. Aslam. 2021. Facial reshaping operator for controllable face beautification. Expert Systems with Applications 167: 114067 .
- Hu, Y., H.P. Shum, and E.S. Ho. 2020. Multi-task deep learning with optical flow features for self-driving cars. IET intelligent transport systems. .
- Jeon, M., D. Park, J. Lee, H. Jeon, M. Ko, S. Kim, Y. Choi, A.C. Tan, and J. Kang. 2019. Resimnet: drug response similarity prediction using siamese neural networks. Bioinformatics 35(24): 5249–5256 .
- Jiang, W. and W. Wang 2017. Face detection and recognition for home service robots with end-to-end deep neural networks. In 2017 IEEE International Conference on Acoustics, Speech and Signal Processing (ICASSP), pp. 2232–2236. IEEE.
- Junior, J.M., A. Tommaselli, and M. Moraes. 2016. Calibration of a catadioptric omnidirectional vision system with conic mirror. ISPRS Journal of Photogrammetry and Remote Sensing 113: 97–105 .
- Khaliq, A., S. Ehsan, Z. Chen, M. Milford, and K. McDonald-Maier. 2019. A holistic visual place recognition approach using lightweight CNNs for significant viewpoint and appearance changes. IEEE Transactions on Robotics 36(2): 561–569 .
- Korrapati, H. and Y. Mezouar. 2017. Multi-resolution map building and loop closure with omnidirectional images. Autonomous Robots 41(4): 967–987 .
- Krizhevsky, A., I. Sutskever, and G.E. Hinton. 2012. Imagenet classification with deep convolutional neural networks. Advances in neural information processing systems 25: 1097–1105 .
- Leyva-Vallina, M., N. Strisciuglio, M. Lopez-Antequera, R. Tylecek, M. Blaich, and N. Petkov. 2019. Tb-places: A data set for visual place recognition in garden environments. IEEE Access 7: 52277–52287 .
- Leyva-Vallina, M., N. Strisciuglio, and N. Petkov 2019. Place recognition in gardens by learning visual representations: data set and benchmark analysis. In International Conference on Computer Analysis of Images and Patterns, pp. 324–335. Springer.
- Leyva-Vallina, M., N. Strisciuglio, and N. Petkov. 2021. Generalized contrastive optimization of siamese networks for place recognition. arXiv

[preprint arXiv:2103.06638](#) .

- Li, R., Q. Liu, J. Gui, D. Gu, and H. Hu. 2017. Indoor relocalization in challenging environments with dual-stream convolutional neural networks. IEEE Transactions on Automation Science and Engineering 15(2): 651–662 .
- Li, Y. and X. Zhang. 2019. Siamvgg: Visual tracking using deeper siamese networks. [arXiv preprint arXiv:1902.02804](#) .
- Lin, J., J. Peng, Z. Hu, X. Xie, R. Peng, et al. 2020. ORB-SLAM, imu and wheel odometry fusion for indoor mobile robot localization and navigation. Academic Journal of Computing & Information Science 3(1) .
- Liu, W., Y. Mo, and J. Jiao 2019. An efficient edge-feature constraint visual SLAM. In Proceedings of the International Conference on Artificial Intelligence, Information Processing and Cloud Computing, pp. 1–7.
- Liu, Y. and H. Zhang 2012. Visual loop closure detection with a compact image descriptor. In 2012 IEEE/RSJ International Conference on Intelligent Robots and Systems, pp. 1051–1056. IEEE.
- Lu, Y. and G. Lu 2019. Deep unsupervised learning for simultaneous visual odometry and depth estimation. In 2019 IEEE International Conference on Image Processing (ICIP), pp. 2571–2575. IEEE.
- Luthardt, S., V. Willert, and J. Adamy 2018. LLama-SLAM: Learning high-quality visual landmarks for long-term mapping and localization. In 2018 21st International Conference on Intelligent Transportation Systems (ITSC), pp. 2645–2652. IEEE.
- Ma, L., J. Chen, et al. 2019. Using RGB image as visual input for mapless robot navigation. [arXiv preprint arXiv:1903.09927](#) .
- Moolan-Feroze, O., K. Karachalios, D.N. Nikolaidis, and A. Calway 2019. Improving drone localisation around wind turbines using monocular model-based tracking. In 2019 International Conference on Robotics and Automation (ICRA), pp. 7713–7719. IEEE.
- Nozawa, N., H.P. Shum, Q. Feng, E.S. Ho, and S. Morishima. 2021. 3d car shape reconstruction from a contour sketch using gan and lazy learning. The Visual Computer: 1–14 .
- Organisciak, D., D. Sakkos, E.S. Ho, N. Aslam, and H.P. Shum. 2020. Unifying person and vehicle re-identification. IEEE Access 8: 115673–115684 .
- Parajuli, N., A. Lu, J.C. Stendahl, M. Zontak, N. Boutagy, I. Alkhalil, M. Eberle, B.A. Lin, M. O’Donnell, A.J. Sinusas, et al. 2017. Flow

- network based cardiac motion tracking leveraging learned feature matching. In International Conference on Medical Image Computing and Computer-Assisted Intervention, pp. 279–286. Springer.
- Polvara, R., S. Sharma, J. Wan, A. Manning, and R. Sutton. 2018. Obstacle avoidance approaches for autonomous navigation of unmanned surface vehicles. The Journal of Navigation 71(1): 241–256 .
- Pronobis, A. and B. Caputo. 2009, May. COLD: COsy Localization Database. The International Journal of Robotics Research (IJRR) 28(5): 588–594. <https://doi.org/10.1177/0278364909103912> .
- Raúl Mur-Artal, J.M.M.M. and J.D. Tardós. 2015. ORB-SLAM: A versatile and accurate monocular SLAM system. IEEE Transactions on Robotics. <https://doi.org/10.1109/TRO.2015.2463671> .
- Reinoso, O. and L. Payá. 2020. Special issue on mobile robots navigation. Applied Sciences 10(4): 1317 .
- Rituerto, A., L. Puig, and J.J. Guerrero 2010. Visual SLAM with an omnidirectional camera. In 2010 20th International Conference on Pattern Recognition, pp. 348–351. IEEE.
- Ruan, X., D. Ren, X. Zhu, and J. Huang 2019. Mobile robot navigation based on deep reinforcement learning. In 2019 Chinese control and decision conference (CCDC), pp. 6174–6178. IEEE.
- Sakkos, D., H.P. Shum, and E.S. Ho 2019. Illumination-based data augmentation for robust background subtraction. In 2019 13th International Conference on Software, Knowledge, Information Management and Applications (SKIMA), pp. 1–8. IEEE.
- Sandouk, U. and K. Chen. 2017. Learning contextualized music semantics from tags via a siamese neural network. ACM Transactions on Intelligent Systems and Technology 8(2): 24 .
- Shamsfakhr, F., B.S. Bigham, and A. Mohammadi. 2019. Indoor mobile robot localization in dynamic and cluttered environments using artificial landmarks. Engineering Computations .
- Sharma, P., H. Liu, H. Wang, and S. Zhang 2017. Securing wireless communications of connected vehicles with artificial intelligence. In 2017 IEEE international symposium on technologies for homeland security (HST), pp. 1–7. IEEE.
- Simonyan, K. and A. Zisserman. 2014. Very deep convolutional networks for large-scale image recognition. arXiv preprint arXiv:1409.1556 .

- Sinha, H., J. Patrikar, E.G. Dhekane, G. Pandey, and M. Kothari 2018. Convolutional neural network based sensors for mobile robot relocalization. In 2018 23rd International Conference on Methods & Models in Automation & Robotics (MMAR), pp. 774–779. IEEE.
- Sun, Y., C. Cheng, Y. Zhang, C. Zhang, L. Zheng, Z. Wang, and Y. Wei 2020a. Circle loss: A unified perspective of pair similarity optimization. In Proceedings of the IEEE/CVF Conference on Computer Vision and Pattern Recognition, pp. 6398–6407.
- Sun, Y., C. Cheng, Y. Zhang, C. Zhang, L. Zheng, Z. Wang, and Y. Wei 2020b, June. Circle loss: A unified perspective of pair similarity optimization. In Proceedings of the IEEE/CVF Conference on Computer Vision and Pattern Recognition (CVPR).
- Szegedy, C., W. Liu, Y. Jia, P. Sermanet, S. Reed, D. Anguelov, D. Erhan, V. Vanhoucke, and A. Rabinovich 2015. Going deeper with convolutions. In Proceedings of the IEEE conference on computer vision and pattern recognition, pp. 1–9.
- Tanzmeister, G., J. Thomas, D. Wollherr, and M. Buss 2014. Grid-based mapping and tracking in dynamic environments using a uniform evidential environment representation. In 2014 IEEE International Conference on Robotics and Automation (ICRA), pp. 6090–6095. IEEE.
- Thiolliere, R., E. Dunbar, G. Synnaeve, M. Versteegh, and E. Dupoux 2015. A hybrid dynamic time warping-deep neural network architecture for unsupervised acoustic modeling. In Sixteenth Annual Conference of the International Speech Communication Association.
- Utkin, L.V., V.S. Zaborovsky, and S.G. Popov. 2017. Siamese neural network for intelligent information security control in multi-robot systems. Automatic Control and Computer Sciences 51(8): 881–887 .
- Wang, Y., T. Bao, C. Ding, and M. Zhu 2017. Face recognition in real-world surveillance videos with deep learning method. In 2017 2nd International Conference on Image, Vision and Computing (ICIVC), pp. 239–243. IEEE.
- Weinzaepfel, P., G. Csurka, Y. Cabon, and M. Humenberger 2019. Visual localization by learning objects-of-interest dense match regression. In Proceedings of the IEEE/CVF Conference on Computer Vision and Pattern Recognition, pp. 5634–5643.
- Xu, S., W. Chou, and H. Dong. 2019. A robust indoor localization system integrating visual localization aided by CNN-based image retrieval with monte carlo localization. Sensors 19(2): 249 .

- Yin, H., L. Tang, X. Ding, Y. Wang, and R. Xiong 2018. Locnet: Global localization in 3d point clouds for mobile vehicles. In 2018 IEEE Intelligent Vehicles Symposium (IV), pp. 728–733. IEEE.
- Zaki, H.F., F. Shafait, and A. Mian. 2019. Viewpoint invariant semantic object and scene categorization with RGB-D sensors. Autonomous Robots 43(4): 1005–1022 .
- Zeng, A., S. Song, K.T. Yu, E. Donlon, F.R. Hogan, M. Bauza, D. Ma, O. Taylor, M. Liu, E. Romo, et al. 2018. Robotic pick-and-place of novel objects in clutter with multi-affordance grasping and cross-domain image matching. In 2018 IEEE international conference on robotics and automation (ICRA), pp. 3750–3757. IEEE.
- Zhang, Z. and H. Peng 2019. Deeper and wider siamese networks for real-time visual tracking. In Proceedings of the IEEE/CVF Conference on Computer Vision and Pattern Recognition, pp. 4591–4600.
- Zhao, Q., B. Zhang, S. Lyu, H. Zhang, D. Sun, G. Li, and W. Feng. 2018. A CNN-SIFT hybrid pedestrian navigation method based on first-person vision. Remote Sensing 10(8): 1229 .
- Zheng, W., L. Yang, R.J. Genco, J. Wactawski-Wende, M. Buck, and Y. Sun. 2019. Sense: Siamese neural network for sequence embedding and alignment-free comparison. Bioinformatics 35(11): 1820–1828 .
- Zhong, F., S. Wang, Z. Zhang, and Y. Wang 2018. Detect-SLAM: Making object detection and SLAM mutually beneficial. In 2018 IEEE Winter Conference on Applications of Computer Vision (WACV), pp. 1001–1010. IEEE.